Cellular/Molecular

The Role of BK_{Ca} Channels in Electrical Signal Encoding in the Mammalian Auditory Periphery

Dominik Oliver,[1] Annette M. Taberner,[2,3] Henrike Thurm,[1] Matthias Sausbier,[4] Claudia Arntz,[4] Peter Ruth,[4] Bernd Fakler,[1] and M. Charles Liberman[2,3]

[1]Physiologisches Institut, Universität Freiburg, D-79104 Freiburg, Germany, [2]Eaton-Peabody Laboratory, Massachusetts Eye and Ear Infirmary, Boston, Massachusetts 02114, [3]Program in Speech and Hearing Bioscience and Technology, Harvard University–Massachusetts Institute of Technology, Cambridge, Massachusetts 02139, and [4]Department of Pharmacology and Toxicology, Universität Tübingen, D-72074 Tübingen, Germany

Large-conductance voltage- and Ca^{2+}-activated K^+ channels (BK_{Ca}) are involved in shaping spiking patterns in many neurons. Less is known about their role in mammalian inner hair cells (IHCs), mechanosensory cells with unusually large BK_{Ca} currents. These currents may be involved in shaping the receptor potential, implying crucial importance for the properties of afferent auditory signals.

We addressed the function of BK_{Ca} by recording sound-induced responses of afferent auditory nerve (AN) fibers from mice with a targeted deletion of the pore-forming α-subunit of BK_{Ca} ($BK\alpha^{-/-}$) and comparing these with voltage responses of current-clamped IHCs. BK_{Ca}-mediated currents in IHCs were selectively abolished in $BK\alpha^{-/-}$, whereas cochlear physiology was essentially normal with respect to cochlear sensitivity and frequency tuning.

$BK\alpha^{-/-}$ AN fibers showed deteriorated precision of spike timing, measured as an increased variance of first spike latency in response to tone bursts. This impairment could be explained by a slowed voltage response in the presynaptic IHC resulting from the reduced K^+ conductance in the absence of BK_{Ca}. Maximum spike rates of AN fibers were reduced nearly twofold in $BK\alpha^{-/-}$, contrasting with increased voltage responses of IHCs. In addition to presynaptic changes, which may be secondary to a modest depolarization of $BK\alpha^{-/-}$ IHCs, this reduction in AN rates suggests a role of BK_{Ca} in postsynaptic AN neurons, which was supported by increased refractory periods.

In summary, our results indicate an essential role of IHC BK_{Ca} channels for precise timing of high-frequency cochlear signaling as well as a function of BK_{Ca} in the primary afferent neuron.

Key words: calcium-activated potassium channel; Maxi-K; inner ear; hearing; frequency tuning; adaptation

Introduction

Action potential (AP) waveforms and spiking patterns of neurons are shaped by K^+ channels activated during single spikes or spike trains via depolarization or subsequent elevation of cytoplasmic Ca^{2+} (Connor and Stevens, 1971; Golding et al., 1999; Lien and Jonas, 2003). In particular, BK_{Ca} channels, which are large-conductance, voltage- and Ca^{2+}-dependent K^+ channels, play a prominent role in determining the AP phenotype in many neurons (Vergara et al., 1998; Shao et al., 1999; Faber and Sah, 2003). In nonmammalian auditory hair cells, BK_{Ca} contributes to electrical frequency tuning in the absence of APs (Art and Fettiplace, 1987; Fettiplace and Fuchs, 1999). However, less is known about the impact of BK_{Ca} on electrical signaling in other nonspiking cells, such as retinal neurons (Sakaba et al., 1997; Mitra and Slaughter, 2002) or mechanosensory hair cells of the mammalian ear, despite strong expression of BK_{Ca} in these cells (Skinner et al., 2003; Vigh et al., 2003). Mammalian inner hair cells (IHCs) are a useful system to study the role of BK_{Ca} in nonregenerative electrical signaling operating in a frequency range far beyond that of usual neurons. IHCs generate graded receptor potentials (RPs) and have large outward-rectifying K^+ currents that are supposed to contribute to shaping of the RP (Kros, 1996; Zeddies and Siegel, 2004). The major current component is carried by BK_{Ca} channels (Thurm et al., 2005). RPs of IHCs consist of a depolarizing direct current (DC) component and an oscillating alternating current (AC) component (Russell and Sellick, 1978; Dallos, 1985). Whereas the DC component encodes stimulus levels, information on the phase of the auditory stimulus is contained only in the AC component (Johnson, 1980; Palmer and Russell, 1986). The RP controls transmitter release onto the dendrites of the primary auditory neurons, which finally carry APs along the auditory nerve (AN) to the brainstem. The demand placed on all stages within this sensory pathway is to encode a large dynamic range of sound pressure amplitudes with high temporal precision.

In nonmammalian auditory hair cells, frequency selectivity is achieved by electrical resonance, arising from interaction of BK_{Ca} and voltage-gated Ca^{2+} channels (Art and Fettiplace, 1987; Fettiplace and Fuchs, 1999). Mammalian IHCs, in contrast, lack electrical resonance (Kros, 1996), suggesting a role for BK_{Ca} other

Received Nov. 17, 2005; revised April 24, 2006; accepted April 24, 2006.

This work was supported by Deutsche Forschungsgemeinschaft Grants Fa 332/5-1 (B.F.) and Ru 571/4-2 (P.R.) and National Institute on Deafness and Other Communication Disorders Grants RO1 DC00188 and P30 DC005209 (M.C.L.).

Correspondence should be addressed to Dr. Dominik Oliver, Physiologisches Institut, Universität Freiburg, Hermann-Herder-Strasse 7, 79104 Freiburg, Germany. E-mail: dominik.oliver@physiologie.uni-freiburg.de.

DOI:10.1523/JNEUROSCI.1047-06.2006

 0270-6474/06/266181-09$15.00/0

than frequency tuning. It is known that BK_{Ca} contributes to maturation of the electrical phenotype of IHCs (Kros et al., 1998) and that gross auditory potentials are affected by intracochlear perfusion of BK_{Ca} blockers (Skinner et al., 2003). However, the role of BK_{Ca} for electrical signal encoding in the mammalian cochlea has not been addressed directly.

We approached this issue by recording from IHCs and AN fibers from mice lacking the pore-forming α-subunit of BK_{Ca} ($BK\alpha^{-/-}$). Loss of the BK_{Ca} current resulted in markedly altered amplitudes and time course of the voltage responses of the IHCs, highlighting the importance of BK_{Ca} for shaping the RP. *In vivo* recordings from AN fibers revealed corresponding changes of the downstream afferent signals. Notably, temporal precision of AN spiking was reduced in $BK\alpha^{-/-}$, matching the slowing of voltage signals in IHCs.

Materials and Methods

Patch-clamp recordings from IHCs. Experiments were performed on homozygous $BK\alpha^{-/-}$ and $BK\alpha^{+/+}$ 129svj inbred littermates (Ruttiger et al., 2004) according to institutional guidelines at the University of Freiburg.

Apical cochlear turns of mice (22–30 d after birth) were prepared as described previously (Oliver et al., 2000). Briefly, animals were anesthetized with isoflurane and killed by decapitation, and the cochleae were dissected. After removal of the cochlear bone, the apical cochlear turn was separated from the modiolus. Stria vascularis and tectorial membrane were stripped off. This whole-mount preparation was placed into an experimental chamber continuously perfused with standard extracellular solution (in mM: 144 NaCl, 5.8 KCl, 1.3 $CaCl_2$, 0.9 $MgCl_2$, 10 HEPES, 0.7 Na_2HPO_4, and 5.6 glucose, pH adjusted to 7.4 with NaOH).

Voltage-clamp recordings were done with Axopatch 200B or Multiclamp 700A amplifiers (Molecular Devices, Union City, CA) at room temperature (20–24°C). Currents were low-pass filtered at 2–10 kHz and sampled at 25 kHz. Electrodes were pulled from quartz glass and filled with a KCl-based intracellular solution (in mM: 135 KCl, 3.5 $MgCl_2$, 5 EGTA, 5 HEPES, and 2.5 Na_2ATP, pH adjusted to 7.3 with HCl) and had initial resistances of 1.2–2.5 MΩ. For measurement of currents through Ca^{2+} channels, KCl was replaced by CsCl and 10 mM 4-AP was added. During whole-cell measurements, series resistance (R_s) was typically 2–5 MΩ. Careful series resistance compensation (90–95%) was applied during all whole-cell experiments, and voltages were corrected off-line for errors attributable to residual R_s. Voltages are presented without correction for liquid junction potential (−4 mV).

Current-clamp recordings were done with a Multiclamp 700A that incorporates a fast voltage follower. Bridge balance was applied to cancel voltage drops across the pipette series resistance, and the pipette capacitance neutralization circuit was used to optimize the frequency response (recording time constants <30 μs).

Extracellular solutions were exchanged via a glass capillary (diameter, ~100 μm) placed close to the IHCs. To block BK_{Ca} currents, 100 nM Iberiotoxin (IbTx) was added to the extracellular solution. Residual currents were recorded after application of IbTx for at least 10 min. To measure currents through Ca_v channels, 10 mM extracellular Ba^{2+} replaced $CaCl_2$ (1.3 mM) and 13 mm NaCl.

Data analysis and fitting was performed with IgorPro (WaveMetrics, Lake Oswego, OR) on a Macintosh PowerPC (Apple Computers, Cupertino, CA).

Auditory nerve recordings. Single-fiber recordings were made from the AN in $BK\alpha^{-/-}$ mice and their $BK\alpha^{+/+}$ littermates at ages 7–17 weeks. All animal procedures were approved by the Institutional Animal Care and Use Committee of the Massachusetts Eye and Ear Infirmary. Animals were anesthetized with xylazine (5 mg/kg, i.p.) and urethane (1.32 mg/kg, i.p.), and rectal temperature was maintained near 38°C. The cartilaginous ear canals were removed, the scalp was reflected, the skull was opened, and a semi-cerebellectomy was performed to expose the left cochlear nucleus. Glass microelectrodes filled with 2 M KCl were directed into the AN through the cochlear nucleus. Criteria for distinguishing AN fibers from cochlear nucleus cells have been presented previously (Taberner and Liberman, 2005). In total, recordings were obtained from 57 AN fibers from six $BK\alpha^{-/-}$ mice and from 64 AN fibers from seven $BK\alpha^{+/+}$ mice.

The sound system comprised dual electrostatic sound sources (TDT ED-1; Tucker-Davis Technologies, Gainesville, FL) and a Knowles electret microphone coupled to a probe tube. The sensitivity of the probe-tube microphone was calibrated for frequencies between 1.0 and 73 kHz using a calibrated Brüel and Kjær (Norcross, GA) ¼ inch condenser microphone in a coupler.

Distortion-product otoacoustic emissions (DPOAEs) were monitored throughout the experiments to assess cochlear stability. DPOAEs are created by nonlinearities in the mechanoelectric transduction process, amplified by the somatic motility of outer hair cells (OHCs), and transmitted back to the ear canal in which they can be measured in the ear-canal sound pressure when two pure tones (f_1, f_2) are presented simultaneously. Details of DPOAE measurement have been presented previously (Taberner and Liberman, 2005).

Noise bursts were used as search stimuli. Tone bursts (50 ms duration, 2.5 ms rise fall, and a 10/s repetition rate) were used for all other sound-evoked measures (except phase locking, which used continuous tones). Tuning curves were measured under computer control and represent isorate contours for response of 10 spikes per second (sp/s) > spontaneous rate (SR) (Liberman, 1978). Spontaneous rates were calculated from 10 s samples. Rate-level functions were measured at characteristic frequency (CF) with 10–40 tone bursts per level. Levels (in 5 dB steps) were presented in random order. Rate-level functions (Taberner and Liberman, 2005) were fit in Matlab (MathWorks, Natick, MA). Dynamic range was defined as the difference between sound pressure levels (SPLs) evoking 10 and 90% of the (model fit) maximum driven rate. The variance of the first spike latency (FSL) was extracted from the distribution of spike times for the first spike discharge after each tone burst onset. Relative and absolute refractory periods were estimated from interval histograms as described by Li and Young (1993) computed from responses to tone bursts at CF at 30 dB above threshold, using only spikes occurring during the steady-state response (>20 ms after tone-burst onset).

Data from IHCs and AN recordings are presented as means ± SEM. Two-tailed *t* tests were used to compute statistical significance.

Results

Hair cell measures *in vitro*

IHC currents in $BK\alpha^{-/-}$

When depolarized, IHCs show large outward K^+ currents, composed of a fast and a more slowly activating component (Kros and Crawford, 1990). As shown in Figure 1*A*, the fast component ($I_{K,f}$) was abolished in $BK\alpha^{-/-}$ mice, leaving much smaller residual currents with slower activation kinetics ($I_{K,s}$). Consequently, overall current amplitudes were greatly reduced at all potentials positive to approximately −60 mV (Fig. 1*B*) and, in particular, across the putative physiological working range of IHCs between −60 and −40 mV (Fig. 1*B*, inset). These findings confirmed that $I_{K,f}$ is carried by BK_{Ca} channels and provided the opportunity to analyze electrical signaling in IHCs and AN fibers in the absence of this dominant K^+ conductance.

We first examined whether other ionic conductances of the IHC were affected by the deletion of BK_{Ca}. The slow K^+ current ($I_{K,s}$) can be isolated by blocking $I_{K,f}$/BK_{Ca} with IbTx (Kros et al., 1998; Skinner et al., 2003). As shown in Figure 1, *A* and *B*, currents measured in $BK\alpha^{+/+}$ in the presence of 100 nM IbTx were equal to the residual current in $BK\alpha^{-/-}$ IHCs without IbTx, in both amplitude and voltage dependence, indicating the absence of compensatory upregulation of other outward rectifiers. Similarly, the background currents of the IHCs carried by KCNQ channels ($I_{K,n}$) (Oliver et al., 2003) were not changed in $BK\alpha^{-/-}$ (Fig. 1*C*). The resting potential (V_R) measured in this isolated preparation *in vitro* was indistinguishable between $BK\alpha^{-/-}$ and $BK\alpha^{+/+}$ IHCs (Fig. 1*D*), consistent with previous findings showing that V_R is determined mainly by $I_{K,n}$ *in vitro*

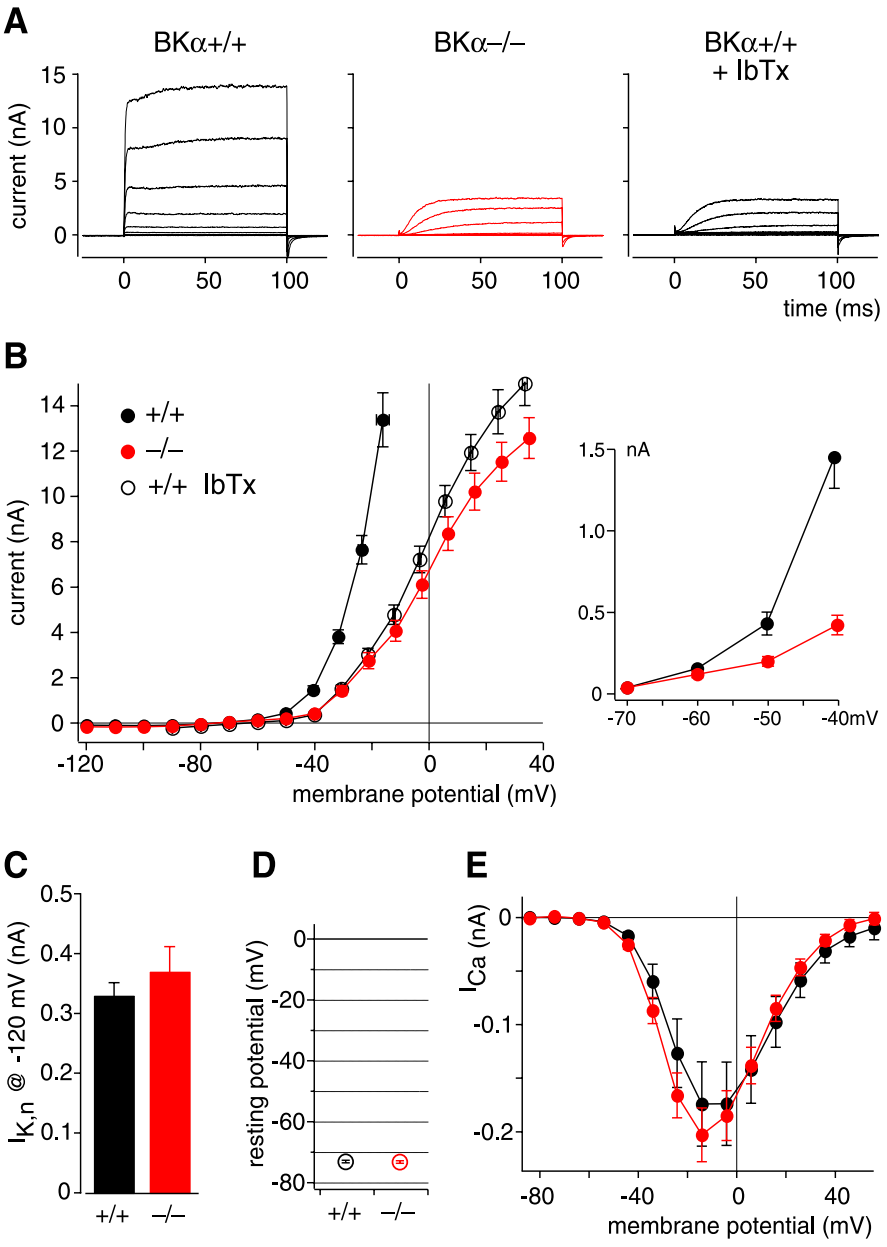

Figure 1. Fast outward K^+ currents ($I_{K,f}$) are selectively abolished in IHCs from BK_{Ca} knock-out mice. ***A***, K^+ currents measured in response to depolarizing voltage steps in nominal increments of 10 mV from a holding potential of −80 mV. Recordings are from a wild-type IHC ($BK\alpha^{+/+}$; left), from a BK_{Ca} knock-out IHC ($BK\alpha^{-/-}$; middle), and from a $BK\alpha^{+/+}$ IHC in the presence of the specific BK_{Ca} blocker IbTx (100 nM; ≥10 min) in the extracellular solution (right). Recordings were made from IHCs in isolated apical turn organs of Corti at 23, 24, and 26 d after birth, respectively. ***B***, Average steady-state current amplitudes from six $BK\alpha^{+/+}$ and 10 $BK\alpha^{-/-}$ IHCs show a large reduction of overall currents. Residual currents of $BK\alpha^{-/-}$ cells are equal to the IbTx-resistant currents of wild-type IHCs ($n = 11$). Currents are plotted against membrane potentials corrected for voltage drops across the residual series resistance (horizontal error bars). Inset, Current amplitudes at the physiological voltage range at enlarged scale. ***C***, The background K^+ current ($I_{K,n}$) is not different between $BK\alpha^{+/+}$ ($n = 9$) and $BK\alpha^{-/-}$ ($n = 7$) IHCs. Currents are quantified as the maximum deactivating inward tail currents at −120 mV after prepulses to voltages between −150 to −60 mV (Oliver et al., 2003). The voltage dependence of this current was also unchanged (half-activating voltage of −95.6 ± 1.7 and −99.5 ± 3.0 mV, respectively). ***D***, Resting membrane potential *in vitro* is equal in $BK\alpha^{+/+}$ ($n = 5$) and $BK\alpha^{-/-}$ ($n = 8$) IHCs. Symbol key in ***B*** also applies to ***D*** and ***E***. ***E***, Calcium currents of IHCs are not affected by ablation of BK_{Ca}. Currents through Ca_v channels from seven $BK\alpha^{+/+}$ and eight $BK\alpha^{-/-}$ IHCs are measured with 10 mM extracellular Ba^{2+} as the charge carrier and with intracellular Cs^+/4-AP and extracellular tetraethylammonium (10 mM) to block all K^+ currents.

(Oliver et al., 2003). We further checked for any alterations in the Ca^{2+} current of the IHCs, because I_{Ca} transforms the voltage signal of the IHCs into a synaptic signal. I_{Ca} was also indistinguishable between $BK\alpha^{-/-}$ and $BK\alpha^{+/+}$ (Fig. 1*E*).

Thus, $I_{K,f}$ was selectively abolished and other conductances of IHCs were not changed by the deletion of BK_{Ca}. The present $BK\alpha^{-/-}$ model appeared well suited to examine the role of BK_{Ca} for cochlear signal processing.

Voltage responses of the IHC

We next examined the consequences of deletion of BK_{Ca} for the voltage signals of the IHC in current-clamp mode. Whereas in $BK\alpha^{+/+}$ IHCs step currents elicited fast and nearly time-invariant voltage responses, the voltage waveforms in $BK\alpha^{-/-}$ were markedly changed (Fig. 2*A*). Voltage excursions were much larger in $BK\alpha^{-/-}$ IHCs and exhibited a prominent time-dependent relaxation, presumably resulting from the slow activation of the delayed rectifier $I_{K,s}$. Figure 2*B* shows that, in addition to peak responses, steady-state voltages were larger in IHCs from $BK\alpha^{-/-}$.

Moreover, the speed of the voltage response was markedly affected by the loss of BK_{Ca}. As shown in Figure 2*C*, the membrane time constant was nearly twofold larger in $BK\alpha^{-/-}$ IHCs at their *in vitro* resting potential. The faster voltage response in $BK\alpha^{+/+}$ is consistent with the larger overall conductance in the presence of BK_{Ca}, which speeds up the membrane time constant of the IHC. At a more physiological membrane potential of −58 mV (see below), the difference in membrane time constant between $BK\alpha^{+/+}$ and $BK\alpha^{-/-}$ was even more pronounced, being approximately threefold slowed by deletion of BK_{Ca} (Fig. 2*C*). This suggested that BK_{Ca} supplies a larger fraction of the overall conductance at this voltage.

In vivo, the RP is elicited by mechano-electrical transduction currents that are evoked by sinusoidal deflection of the stereociliary bundle. Because of the highly asymmetric transducer function (Kros et al., 1992; Kros, 1996) (supplemental Fig. 1, available at www.jneurosci.org as supplemental material) and the low-pass filtering characteristics of the cell membrane, the RP of IHCs consists of an oscillatory AC component on top of a depolarizing DC potential (Palmer and Russell, 1986). The increased input resistance and membrane time constants in the absence of BK_{Ca} predict that the AC response should be reduced whereas the DC component should be increased, similar to the response to current steps in $BK\alpha^{-/-}$ IHCs. When AC currents were injected, shaped according to the transducer characteristics, reduced AC components and increased DC components were observed in the voltage responses of $BK\alpha^{-/-}$ IHCs, qualitatively supporting this prediction (supplemental Fig. 1, available at www.jneurosci.org as supplemental material).

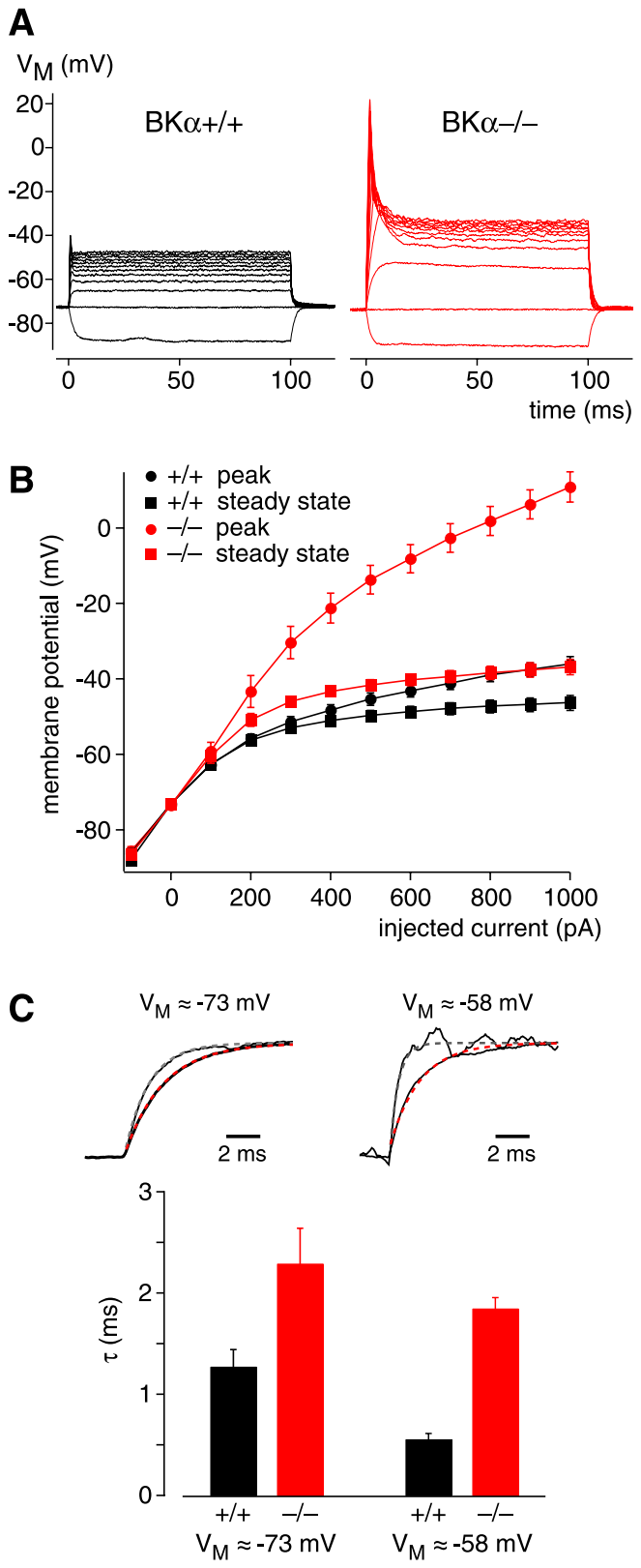

Figure 2. Voltage responses of $BK\alpha^{-/-}$ IHCs have increased amplitudes and slowed time constants. ***A***, Voltage responses measured from current-clamped IHCs show increased onset and steady-state amplitudes in $BK\alpha^{-/-}$ IHCs. Voltage responses were elicited by current steps in 100 pA increments. ***B***, Average peak and steady-state voltage responses measured from five $BK\alpha^{+/+}$ and seven $BK\alpha^{-/-}$ IHCs as in ***A*** are displayed as a function of the current step. Correspondence between genotype and symbol is shown in the key. ***C***, Top, Onset of voltage responses of IHCs to a 100 pA current step recorded from $BK\alpha^{+/+}$ IHCs (gray) and $BK\alpha^{-/-}$ IHCs (red). Recordings were obtained from either resting potential (left) or cells held close to −58 mV, a voltage probably similar to the *in vivo* resting potential (right; see Results). Non-averaged voltage traces are plotted normalized to maximum. Time constants are derived from monoexponential fits (dashed lines) to the voltage onsets. Bottom, Time constants were significantly slower in $BK\alpha^{-/-}$ IHCs than in $BK\alpha^{+/+}$, both for the *in vitro* resting potential ($n = 7$ and 5 IHCs for $BK\alpha^{-/-}$ and $BK\alpha^{+/+}$, respectively; $p < 0.05$) and at −58 mV ($n = 3$ each; $p < 0.001$).

It has been suggested that the hair cell resting potential is more depolarized *in vivo* than *in vitro*, because the resting transducer conductance, which is essentially lost on cell isolation, will tend to depolarize the cell (Kros, 1996; Zeddies and Siegel, 2004). Taking a maximum transducer conductance of 13 nS as obtained from neonatal IHCs (Kros, 1996), the fraction of channels open at rest to be 0.1 (Kros, 1996; Zeddies and Siegel, 2004), and a driving force of 145 mV (60 mV V_M plus 85 mV endocochlear potential), we estimate a standing depolarizing current of ~190 pA. The voltage–current relationships from Figure 2*B* show that this current will depolarize the IHC to −57 mV in the presence of BK_{Ca} channels but to −52 mV in IHCs lacking BK_{Ca}. This difference indicates that, in addition to alterations of the RP, the IHC resting potential *in vivo* is slightly depolarized in $BK\alpha^{-/-}$ compared with wild-type IHCs. In adult OHCs, transducer currents are substantially larger than in neonatal OHCs (He et al., 2004). A similar increase in transducer conductance during maturation seems likely for IHCs; therefore, this estimated depolarization of $BK\alpha^{-/-}$ IHCs may be regarded as a lower limit. However, Figure 2*B* shows that BK-dependent depolarization is not larger than 10 mV, even with larger standing mechanoelectric transduction currents of up to 1 nA.

Auditory nerve responses *in vivo*

The above results obtained in the isolated sensory epithelium suggest that BK_{Ca} contributes to the resting potential of the IHC and shapes the RP that occurs during acoustical stimulation *in vivo*. This implies effects of BK_{Ca} on auditory signals downstream of the RP with respect to both amplitude and fine timing. First, the increased voltage responses in the absence of BK_{Ca} may affect encoding of the SPLs in AN afferents. Second, slowed IHC voltage responses at stimulus onset and reduction of the AC component suggest that the temporal precision of AN spike trains may be impaired in the absence of BK_{Ca}-mediated currents. To address these predictions, responses of single AN fibers were measured *in vivo*.

Threshold tuning and spontaneous rates

Integrity of cochlear physiology was monitored as the threshold of individual AN fibers. Mean thresholds of individual AN fibers were slightly higher in $BK\alpha^{-/-}$ than in $BK\alpha^{+/+}$ littermates (15–20 dB); however, there was large threshold overlap in all frequency regions (Fig. 3*A*). Data in Figure 3*A* show thresholds at the CF, i.e., the sensitive "tip" of the tuning curve (inset). The CF indicates where along the mechanically tuned cochlear spiral each AN fiber originates; the threshold at CF is dependent on the cochlear amplification provided by OHCs in that region. Similar results for cochlear sensitivity were obtained by measuring DPOAE thresholds that depend on integrity of the cochlear amplification process upstream of IHC and AN responses (supplemental Fig. 2*A*, available at www.jneurosci.org as supplemental material). The sharpness of frequency tuning, which also depends on OHC function, was not different in the two genotypes (Fig. 3*B*). These data indicate that, despite a slight loss in threshold sensitivity, cochlear physiology is not severely impaired in $BK\alpha^{-/-}$ mice, allowing

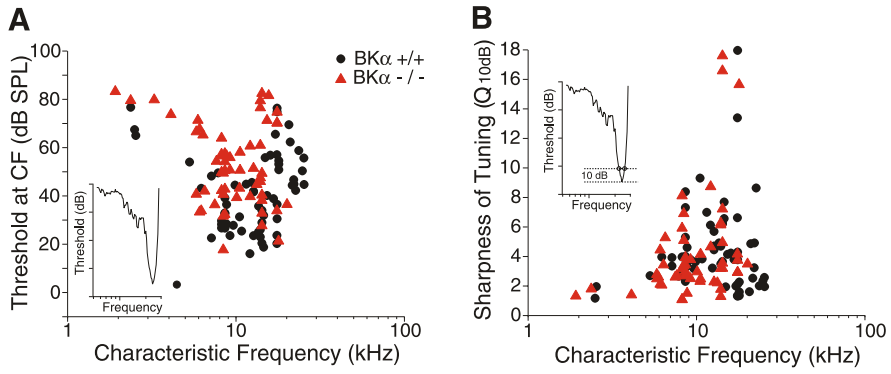

Figure 3. Thresholds in the $BK\alpha^{-/-}$ mice are slightly elevated, but tuning properties of AN fibers are not altered. ***A***, Cochlear sensitivity was measured via isoresponse contours for AN fibers. Thresholds show a large overlap between individual AN fibers of wild-type and $BK\alpha^{-/-}$ ears with a slight elevation of the average threshold in $BK\alpha^{-/-}$. As seen in the inset, each point in this scatter plot represents threshold at the characteristic frequency of an AN. ***B***, Sharpness of tuning of AN fibers shows no differences between $BK\alpha^{-/-}$ versus $BK\alpha^{+/+}$ ears. Tuning is measured as "$Q_{10\ dB}$," i.e., the characteristic frequency divided by the bandwidth at 10 dB above threshold. Symbol key in ***A*** also applies to ***B***.

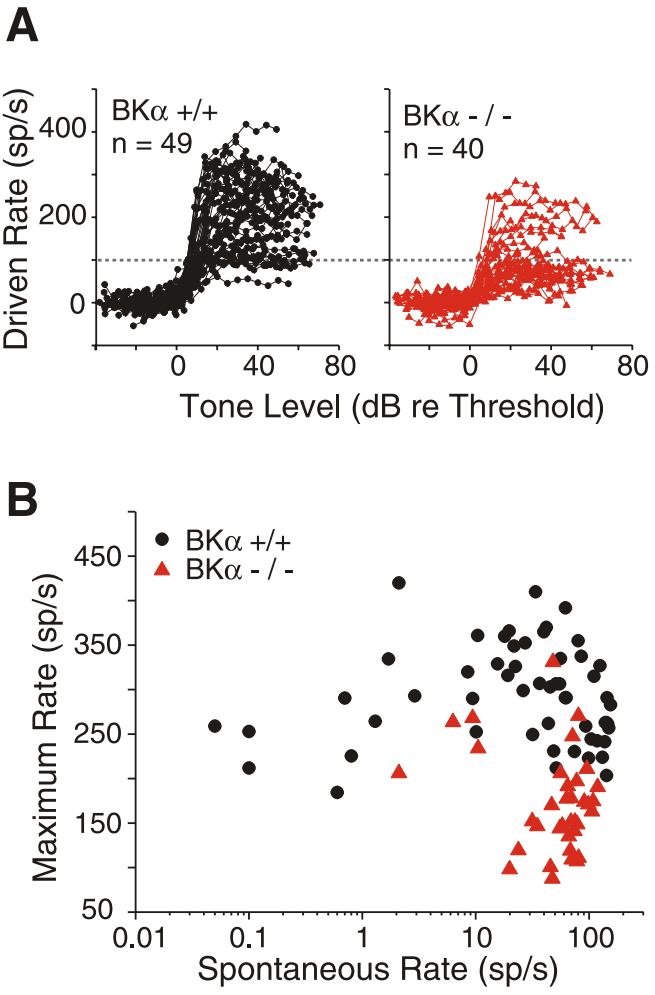

Figure 4. AN fibers from $BK\alpha^{-/-}$ ears show a decrease in saturated discharge rates. ***A***, All rate-versus-level functions for AN fibers with high spontaneous discharge rates (>1 sp/s) are superimposed for $BK\alpha^{+/+}$ (black) and $BK\alpha^{-/-}$ (red) ears. The position of each function along the *x*-axis is normalized to the model-fit threshold (see Materials and Methods). The "driven rate" (*y*-axis) is defined as the average discharge rate minus the spontaneous rate. ***B***, Maximum rates are plotted versus SR for all fibers from $BK\alpha^{-/-}$ and $BK\alpha^{+/+}$ ears. Fibers with spontaneous rate of 0 are plotted as 0.05 sp/s. Correspondence between symbol type and genotype is shown in the key. Maximum rates are derived from the model-fit data (see Materials and Methods) and are larger than the driven-rate values in ***A***, because spontaneous rates have not been subtracted out.

a meaningful assessment of the function of BK_{Ca} in electrical signaling by IHCs and AN fibers *in vivo*.

AN fibers discharge spontaneously in the absence of sound. A single IHC is innervated by fibers with high-SR and by low-SR fibers (Liberman, 1982). Among normal mouse AN fibers, SR ranges from 0 to 160 sp/s: the frequency distribution is skewed, with a low-rate peak and a long high-rate tail (Taberner and Liberman, 2005). Loss of BK_{Ca} channels reduced the relative size of the low-rate peak: fibers with SR <5 sp/s made up 18% of $BK\alpha^{+/+}$ fibers sampled [a proportion similar to that in CBA/CaJ mice (Taberner and Liberman, 2005)] but only 4% of fibers from the $BK\alpha^{-/-}$ ears. Because spontaneous activity is driven by synaptic transmitter release from IHCs and is modulated by changes in IHC membrane potential (Sewell, 1984; Siegel and Relkin, 1987), a reduction in number of low-SR fibers is consistent with the inferred IHC depolarization in $BK\alpha^{-/-}$ ears. However, such depolarization should increase the mean rate of the high-SR population as well, and such a change was not observed. Alternatively, the relative reduction in low-SR fibers may arise because these fibers normally have high thresholds (Liberman, 1978), and the decreased sensitivity in $BK\alpha^{-/-}$ may cause low-SR thresholds to exceed the level of the search stimulus and thus elude detection.

Dynamic range and maximum discharge rates

Although the dynamic range of the auditory system spans >120 dB from the threshold of hearing to the threshold of pain, individual mouse AN fibers typically have dynamic ranges of only 10–30 dB (Taberner and Liberman, 2005); thus, recruitment of fibers with differing thresholds must be invoked to explain the full span. Because dynamic range is normally higher in low-SR fibers than in high-SR fibers (supplemental Fig. 2*B*, available at www.jneurosci.org as supplemental material) (Taberner and Liberman, 2005), measured dynamic ranges were matched for SR. Despite the changes in the voltage response amplitudes in IHCs (Fig. 2), there was no significant effect of genotype: dynamic ranges for high-SR (>10 sp/s) fibers averaged 14.1 ± 1.0 dB in $BK\alpha^{-/-}$ ($n = 37$) versus 14.8 ± 0.7 dB ($n = 43$) in $BK\alpha^{+/+}$.

In contrast to this small change in dynamic range, sound-evoked discharge rates were strongly affected by deletion of BK_{Ca}. As seen in superimposed rate-versus-level functions (Fig. 4*A*), most $BK\alpha^{+/+}$ fibers saturated at driven rates >100 sp/s, whereas most $BK\alpha^{-/-}$ fibers had driven rates <100 sp/s. The differences are even more striking when maximum rate is plotted and fiber SR is considered (Fig. 4*B*): among high-SR fibers, there is little overlap in maximum saturated rate between the two genotypes. Maximum discharge rate in high-SR fibers averaged 297 ± 8.0 sp/s in $BK\alpha^{+/+}$ ($n = 40$) versus 165 ± 8.4 sp/s in $BK\alpha^{-/-}$ ($n = 37$). The differences were highly significant ($p \ll 0.0001$).

The decrease in spike rates was surprising given that loss of BK_{Ca} increased steady-state voltages and initial voltage excursions for large stimuli in the IHC (Fig. 2*A*,*B*). To better understand the mechanisms underlying these changes, we must dissect the average-rate values of Figure 4 into their onset and

steady-state components. As seen in poststimulus time histograms (Fig. 5*A*), there is a pronounced adaptation in AN response to tone bursts (Kiang et al., 1965; Taberner and Liberman, 2005): an onset peak, with instantaneous rate as high as 1000 sp/s, decays to a lower steady-state rate (Smith et al., 1983). Although both onset rates and steady-state rates were reduced in $BK\alpha^{-/-}$, the onset-rate reduction (Fig. 5*B*) was smaller than the steady-state rate reduction (Fig. 5*C*). As a result, adaptation appears greater in the $BK\alpha^{-/-}$ histograms (Fig. 5*A*). As discussed below, the decreased onset rates may be well explained by the slower onset of the RP attributable to the longer membrane time constant in IHCs in the absence of BK_{Ca}. The decrease in steady-state rates may be attributable, in part, to changes in AN refractory periods (see below).

Temporal precision

In IHCs, temporal properties of the RP were impaired by loss of BK_{Ca}. Two measures can be used to gauge corresponding effects of BK_{Ca} deletion on temporal precision in the AN: (1) the degree of phase locking to a low-frequency tone, and (2) the temporal jitter in the first spike evoked by a tone burst.

Phase locking of spike times to the cycles of a low-frequency (<4 kHz) tone is a key feature of the mammalian AN (Palmer and Russell, 1986). Because phase locking, also termed "synchrony," requires the AC component of the RP of the IHC, the increase in membrane time constant observed in IHC recordings (Fig. 2) (supplemental Fig. 1, available at www.jneurosci.org as supplemental material) suggests impairment of synchrony in the absence of BK_{Ca}. Unfortunately, the mouse is a high-frequency mammal, and very few ANs respond to frequencies below 4 kHz at non-traumatic sound levels (Taberner and Liberman, 2005); thus, our synchrony database is limited. Consistent with expectations, synchronization indices from $BK\alpha^{-/-}$ were smaller than in $BK\alpha^{+/+}$ (supplemental Fig. 2*C*, available at www.jneurosci.org as supplemental material); however, the data set is too small to meaningfully assess the significance of this difference.

In contrast, precision in the timing of the first spike in response to a tone stimulus at CF could be assessed for many AN fibers. Temporal precision was quantified as the variance of the FSL distribution. As shown in Figure 5*D*, FSL variances were altered by BK_{Ca} deletion: although some fibers in BKα null ears showed normal FSL variance, the majority showed increased variance by up to two orders of magnitude. In wild-type ears, onset rate is correlated with the FSL variance (Fig. 5*D*): the lower the FSL variance, the more spikes fall in the same bin of the poststimulus time histogram (Fig. 5*A*) and the higher the onset rate. Accordingly, the $BK\alpha^{-/-}$ fibers with normal variance also showed normal onset rates and vice versa.

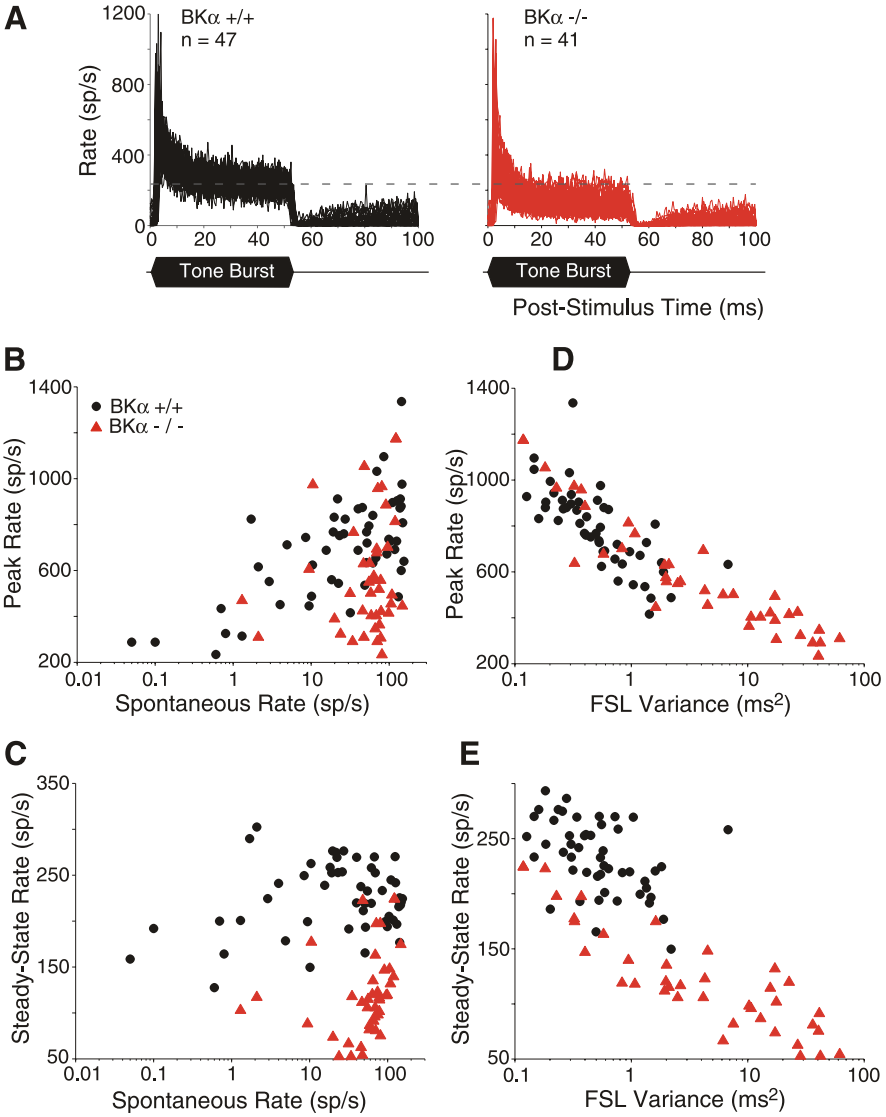

Figure 5. Both onset rate and steady-state rate are diminished in the AN of $BK\alpha^{-/-}$ mice. ***A***, Poststimulus time histograms for responses to tone bursts at the CF superimposed from all AN fibers with high spontaneous rates (>1 sp/s) from the genotypes indicated. The tone-burst stimuli were 50 ms in duration. Dashed line indicates mean steady-state rates from wild-type fibers. ***B***, Peak rates were calculated as the maximum value from the poststimulus time histogram divided by the bin width (0.5 ms). Fibers with spontaneous rate of 0 were plotted as 0.05 sp/s. ***C***, Steady-state rate was calculated as the average rate for the final 15 ms of the tone burst. ***D***, ***E***, The variance of the FSL was extracted from the distribution of spike times for the first spike discharge after each tone-burst onset. Peak and steady-state rates are measured as described for ***B*** and ***C***, respectively. The analyses of spike rates and spike timing in this figure are based on spike times measured in response to 200–300 tone bursts at the characteristic frequency, presented 30 dB above threshold.

The loss of temporal accuracy in AN onset times is consistent with the increased membrane time constants of IHCs that lead to slowed onset of presynaptic voltage signals (Fig. 2*C*,*D*) in $BK\alpha^{-/-}$. This indicates that BK_{Ca} in the sensory IHC is required for high temporal precision in the postsynaptic afferent pathway. However, the maintenance of normal FSL variance in a subset of $BK\alpha^{-/-}$ fibers has no obvious correlate in the IHC data: this "normal" subset was not concentrated in any particular CF region nor in particular animals, i.e., every animal showed a mixture of normal and abnormal temporal responses. A possible explanation for this variation of onset precision could be a variable amplitude of $I_{K,n}$/KCNQ currents in the IHC (Marcotti et al.,

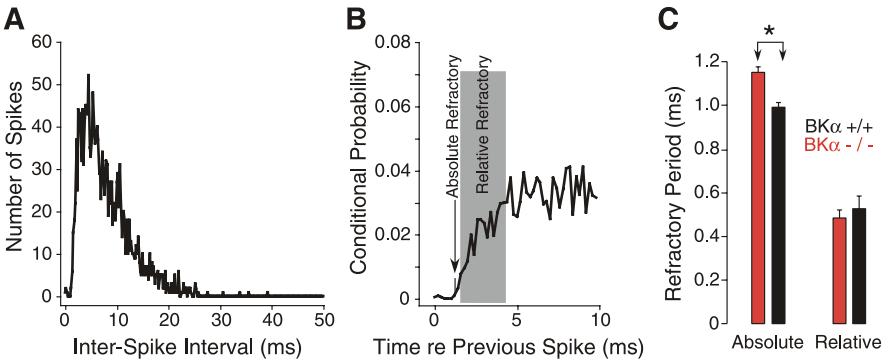

Figure 6. The absolute refractory period is prolonged in AN fibers of $BK\alpha^{-/-}$ mice. Estimates of absolute and relative refractory periods were extracted from conditional probability histograms (Li and Young, 1993) based on spike times seen in response to tone bursts at the characteristic frequency. ***A***, First, interspike interval histograms were computed using only spikes occurring during the steady-state response (>20 ms after tone burst onset). ***B***, The "hazard function" plots the conditional probability of discharge as a function of the time since the previous spike. For additional details, see text. ***C***, Mean ± SEM values of absolute and relative refractory periods for all AN fibers sampled in the three groups of mice. The difference between absolute refractory periods in $BK\alpha^{-/-}$ and $BK\alpha^{+/+}$ was highly significant (*$p = 0.00002$, two-tailed *t* test).

2003), which are active at the resting potential and may improve the membrane time constant of the IHC in the absence of BK_{Ca} (Oliver et al., 2003).

Refractory periods in auditory nerve fibers

The marked decrease of (postsynaptic) steady-state AN spike rates (129 ± 7 vs 235 ± 7 sp/s for $BK\alpha^{-/-}$ and $BK\alpha^{+/+}$, respectively) (Fig. 5*C*) stands in contrast to the increase of (presynaptic) voltage responses in the isolated IHC (Fig. 2). Moreover, whereas decreased steady-state rates in $BK\alpha^{-/-}$ fibers were correlated with decreased first spike precision (Fig. 5*E*) indicative of a common, possibly presynaptic origin, fibers with normal spike timing still had reduced steady-state rates compared with $BK\alpha^{+/+}$ fibers (Fig. 5*E*). Thus, an additional mechanism appears to contribute to the decrease in spike rates. This mechanism may be postsynaptic given that spiral ganglion neurons may contain BK_{Ca} channels (Skinner et al., 2003; Hafidi et al., 2005) and loss of BK_{Ca} channels can decrease neuronal spike rates (Sausbier et al., 2004).

We therefore investigated whether loss of BK_{Ca} in the postsynaptic AN fibers contributed to the decrease in sound-evoked rates in $BK\alpha^{-/-}$ mice. To this end, we computed absolute and relative refractory periods from spike interval distributions in responses to tone bursts at the CF (Li and Young, 1993). To estimate refractory periods, a histogram of interspike intervals is created (Fig. 6*A*) using only spikes from the steady-state portion of the response (i.e., 20–50 ms after tone-burst onset). From this histogram, the conditional probability of response as a function of time since the previous spike is computed (Fig. 6*B*): conditional probability at each time *n*, equals the value of the *n*th bin of the interval histogram (Fig. 6*A*) divided by the sum of all subsequent bins. The absolute refractory period is the smallest interspike time above which the probability is consistently >0; the relative refractory period ends where the conditional probability asymptotes. As shown in Figure 6*C*, there was a modest (~20%) but highly significant ($p = 0.00002$) increase in the absolute refractory period in the $BK\alpha^{-/-}$ ears, without significant change in the relative refractory period. This increased refractory period can explain some, but not all, of the decrease in steady-state rate.

Discussion

Role of BK_{Ca} in signal encoding in the IHC

The key electrical signal of the IHC is the RP driving the afferent synapse, which transforms the signal into spiking activity of the auditory neuron. The present recordings from current-clamped IHCs show that both time course and amplitude of voltage responses were affected by deletion of BK_{Ca}, indicating that RPs are altered *in vivo*. Thus, BK_{Ca} in cochlear IHCs strongly contributes to the waveform of the first electrical sensory signal in the auditory system.

First, the increased amplitudes of voltage responses in the absence of BK_{Ca} are consistent with the strong reduction of outward K^+ current and indicate that BK_{Ca} contributes to compressing the transduction current signal into a relatively small range of voltage excursions. The voltage dependence of IHC BK_{Ca} ($V_{1/2}$ of −44 mV) (Oliver et al., 2003; Marcotti et al., 2004) is ideally suited for this task: near resting potential, little BK_{Ca}-mediated K^+ conductance is active, allowing relatively large voltage signals at near-threshold stimuli. With increasing stimuli, fast activation of BK_{Ca} leads to a stronger attenuation of the RP (Fig. 2*A*).

Second, the reduction of K^+ conductance led to an increased membrane time constant at resting potential, which slowed the onset of the voltage responses (Fig. 2*C*,*D*). Activation of BK_{Ca} during the depolarizing phase of the RP may further sharpen the time course at stimulus onset, suggesting that the rapid activation kinetics on the order of 100 μs (Kros and Crawford, 1990; Marcotti et al., 2004) are critical for precise timing at RP onset. Indeed, the kinetics of BK_{Ca} in IHCs are faster than any K_v-type delayed rectifier (Coetzee et al., 1999). Accordingly, activation of the remaining outward rectifier $I_{K,s}$ in $BK\alpha^{-/-}$ resulted in delayed repolarization. The longer membrane time constant should further attenuate the AC component of the RP in $BK\alpha^{-/-}$ at stimulus frequencies above a few hundred hertz (Palmer and Russell, 1986). Injection of a 2 kHz AC current shaped according to transducer characteristics indeed showed selective degradation of the AC component on loss of BK_{Ca} (supplemental Fig. 1, available at www.jneurosci.org as supplemental material). Because the AC RP carries phase information of the auditory stimulus (Palmer and Russell, 1986), the BK_{Ca} channel must also contribute to encoding this temporal feature of auditory stimuli.

Role of BK_{Ca} in AN response and auditory processing

Despite loss of BK_{Ca}, many properties of AN fibers were not significantly altered, including (1) the range of spontaneous rates, (2) the dynamic range of individual fibers, and (3) the shapes of tuning curves. The apparent lack of change in spontaneous rates is not inconsistent with an inferred small degree of resting IHC depolarization given that such a small change in the IHC would be difficult to detect in a population study such as performed here. The unaltered dynamic ranges of single AN fibers is unexpected given the steeper rise of the DC RP in the IHC with increasing current injection. However, the dynamic ranges of normal mouse AN fibers are much smaller than those in other commonly studied mammals; thus, our ability to detect a fractional decrease from a baseline value of only 14 dB (Taberner and Liberman, 2005) may have been limited by the relatively coarse step size (5 dB) in our rate-level assay. The normality of tuning curve shapes in the $BK\alpha^{-/-}$ mice is sig-

nificant because it indicates that, in the mammalian ear, BK_{Ca} does not play the same key role in establishing frequency selectivity as in nonmammalian vertebrates. In the latter, BK_{Ca} channels underlie the electrical resonance of hair cells that dominates the frequency selectivity of the ear (Art and Fettiplace, 1987; Fettiplace and Fuchs, 1999). Our results rule out any contribution of IHC BK_{Ca} channels to frequency tuning and agree with the lack of electrical resonance in IHCs (Kros, 1996).

In contrast to these primarily unchanged characteristics, AN physiology was strongly affected by deletion of BK_{Ca} in two respects: first, both peak and steady-state discharge rates recorded in response to saturating tone bursts were decreased; second, temporal precision of spike timing was reduced.

Because $BK\alpha^{-/-}$ mice show impairment of cochlear sensitivity up to 20–30 dB beginning after 8 weeks of age (Ruttiger et al., 2004), a contribution of cochlear pathology to the observed AN phenotype needs consideration. Our present data confirm a modest degree of cochlear dysfunction evident in the DPOAE, which is consistent with OHC dysfunction (Liberman et al., 2002; Lukashkin et al., 2002). However, sharp mechanical frequency tuning critically requires the amplification process provided by OHCs (Kiang et al., 1970; Dallos and Harris, 1978). Because AN tuning was normal in $BK\alpha^{-/-}$, we conclude that OHC pathology was not severe in the age range used. Expression of BK_{Ca} channels was reported in cochlear cell types related to the production of endolymph and the endolymphatic potential (EP) (Shen et al., 2004; Hafidi et al., 2005); therefore, the possibility should be considered that EP, driving the transduction current of the IHC, is reduced in $BK\alpha^{-/-}$. Our AN data indicate that this is not the case. In addition to elevating thresholds, a reduction in EP would also decrease spontaneous rates in AN fibers (Sewell, 1984) by reducing the driving force for the resting transducer current. In $BK\alpha^{-/-}$ AN fibers, spontaneous rates were unchanged or even elevated, arguing against a decrease of the EP in $BK\alpha^{-/-}$. Thus, the changes in AN phenotype are most likely attributable to loss of BK_{Ca} function in the IHC and/or the AN.

The reduction of steady-state rates stands in contrast to the observed increase in IHC RP; thus, other presynaptic or postsynaptic changes have to be considered. Presynaptically, the inferred resting depolarization of IHCs in $BK\alpha^{-/-}$ could contribute in two ways. First, a major determinant of steady-state rate in AN fibers is the degree of depletion of readily releasable synaptic vesicles (Moser and Beutner, 2000; Spassova et al., 2004). A sustained slight depolarization may result in a reduction of the tonically releasable vesicles. Furthermore, depolarization may drive Ca_v channels into inactivation and thus decrease the Ca^{2+} currents that drive transmission. However, Kharkovets et al. (2006) recently reported that weak depolarization did not appreciably reduce IHC Ca^{2+} currents. Alternatively, IHC depolarization may lead to an increased percentage of transducer channels open at rest because of reduced Ca^{2+} influx (Assad et al., 1989; Kennedy et al., 2003). Such transducer adaptation would result in a more symmetrical transfer function and consequently smaller DC potentials. However, IHC depolarization on the order of 10 mV only slightly reduces the driving force for Ca^{2+}, which may be too small to precipitate a relevant shift of the transfer curve (Assad et al., 1989; Kennedy et al., 2003). Postsynaptic effects of BK_{Ca} deletion must also be considered given reports of BK_{Ca} expression in the somata of AN fibers (Skinner et al., 2003; Hafidi et al., 2005) and pharmacological evidence for BK_{Ca} in developing AN neurons (Adamson et al., 2002). Activation of BK_{Ca} during neuronal APs contributes to the afterhyperpolarization, which facilitates repetitive firing by promoting rapid recovery of Na^+ channels from inactivation (Klyachko et al., 2001). In fact, cerebellar Purkinje cells from the $BK\alpha^{-/-}$ mice show reduced afterhyperpolarization and decreased spike rates (Sausbier et al., 2004). The observed 20% increase in absolute refractory period of the $BK\alpha^{-/-}$ ears is consistent with a similar effect of BK_{Ca} in AN fibers.

Although the above mechanisms may also contribute to the decreased onset rates, the onset rate phenotype is consistent with the changes observed in the presynaptic RP. The slowed onset of the RP should reduce peak rates in the presence of spike rate adaptation occurring at millisecond rates and should increase jitter in the timing of the first spike, which in turn lowers peak rate by reducing the number of spikes clustered into the first bin of the histogram.

Our central finding is the reduced precision of spike timing in $BK\alpha^{-/-}$. The increased jitter of the first spike (FSL variance) at the tone-burst onset is well explained by the slowed onset of the IHC RP. Accurate timing of stimulus onset is critical to a variety of signal processing tasks performed by the auditory CNS. For example, the localization of sounds in the horizontal plane can depend on central circuits accurately extracting and comparing the time of arrival of the sound at the two ears (Palmer, 2004). The maximum difference in time of arrival for a mouse-sized head is <30 μs. The detection of incidence angle changes of $<10°$ in many mammals (Fay, 1988) even implies precision in spike timing on the order of 1–2 μs. This impressive precision is embodied as the ability to phase lock AN spikes to the auditory stimulus up to $\sim$4 kHz (Johnson, 1980; Palmer and Russell, 1986). Although phase locking was difficult to assess in the high-frequency ear of the mouse, our data strongly suggest that the high degree of phase locking observed in auditory systems specialized for lower-frequency hearing such as the human ear critically depends on the conductance provided by BK_{Ca} in the IHC.

In conclusion, BK_{Ca} currents in IHCs are key to the impressive temporal precision of the mammalian ear.

References

Adamson CL, Reid MA, Mo ZL, Bowne-English J, Davis RL (2002) Firing features and potassium channel content of murine spiral ganglion neurons vary with cochlear location. J Comp Neurol 447:331–350.

Art JJ, Fettiplace R (1987) Variation of membrane properties in hair cells isolated from the turtle cochlea. J Physiol (Lond) 385:207–242.

Assad JA, Hacohen N, Corey DP (1989) Voltage dependence of adaptation and active bundle movement in bullfrog saccular hair cells. Proc Natl Acad Sci USA 86:2918–2922.

Coetzee WA, Amarillo Y, Chiu J, Chow A, Lau D, McCormack T, Moreno H, Nadal MS, Ozaita A, Pountney D, Saganich M, Vega-Saenz de Miera E, Rudy B (1999) Molecular diversity of K^+ channels. Ann NY Acad Sci 868:233–285.

Connor JA, Stevens CF (1971) Prediction of repetitive firing behaviour from voltage clamp data on an isolated neurone soma. J Physiol (Lond) 213:31–53.

Dallos P (1985) Response characteristics of mammalian cochlear hair cells. J Neurosci 5:1591–1608.

Dallos P, Harris D (1978) Properties of auditory nerve responses in absence of outer hair cells. J Neurophysiol 41:365–383.

Faber ES, Sah P (2003) Ca^{2+}-activated K^+ (BK) channel inactivation contributes to spike broadening during repetitive firing in the rat lateral amygdala. J Physiol (Lond) 552:483–497.

Fay R (1988) Hearing in vertebrates: a psychophysics databook. Worcester, MA: Hefferman.

Fettiplace R, Fuchs PA (1999) Mechanisms of hair cell tuning. Annu Rev Physiol 61:809–834.

Golding NL, Jung HY, Mickus T, Spruston N (1999) Dendritic calcium spike initiation and repolarization are controlled by distinct potassium channel subtypes in CA1 pyramidal neurons. J Neurosci 19:8789–8798.

Hafidi A, Beurg M, Dulon D (2005) Localization and developmental expression of BK channels in mammalian cochlear hair cells. Neuroscience 130:475–484.

He DZ, Jia S, Dallos P (2004) Mechanoelectrical transduction of adult outer hair cells studied in a gerbil hemicochlea. Nature 429:766–770.

Johnson DH (1980) The relationship between spike rate and synchrony in responses of auditory-nerve fibers to single tones. J Acoust Soc Am 68:1115–1122.

Kennedy HJ, Evans MG, Crawford AC, Fettiplace R (2003) Fast adaptation of mechanoelectrical transducer channels in mammalian cochlear hair cells. Nat Neurosci 6:832–836.

Kharkovets T, Dedek K, Maier H, Schweizer M, Khimich D, Nouvian R, Vardanyan V, Leuwer R, Moser T, Jentsch TJ (2006) Mice with altered KCNQ4 K^+ channels implicate sensory outer hair cells in human progressive deafness. EMBO J 25:642–652.

Kiang NY, Moxon EC, Levine RA (1970) Auditory-nerve activity in cats with normal and abnormal cochleas. In: Sensorineural hearing loss. Ciba Found Symp 1970:241–273.

Kiang NYS, Watanabe T, Thomas C, Clark LF (1965) Discharge patterns of single fibers in the cat's auditory nerve. Cambridge, MA: MIT.

Klyachko VA, Ahern GP, Jackson MB (2001) cGMP-mediated facilitation in nerve terminals by enhancement of the spike afterhyperpolarization. Neuron 31:1015–1025.

Kros CJ (1996) Physiology of mammalian cochlear hair cells. In: The cochlea (Dallos P, Popper N, Fay R, eds), pp 318–385. New York: Springer.

Kros CJ, Crawford AC (1990) Potassium currents in inner hair cells isolated from the guinea-pig cochlea. J Physiol (Lond) 421:263–291.

Kros CJ, Rusch A, Richardson GP (1992) Mechano-electrical transducer currents in hair cells of the cultured neonatal mouse cochlea. Proc Biol Sci 249:185–193.

Kros CJ, Ruppersberg JP, Rusch A (1998) Expression of a potassium current in inner hair cells during development of hearing in mice. Nature 394:281–284.

Li J, Young ED (1993) Discharge-rate dependence of refractory behavior of cat auditory-nerve fibers. Hear Res 69:151–162.

Liberman MC (1978) Auditory-nerve response from cats raised in a low-noise chamber. J Acoust Soc Am 63:442–455.

Liberman MC (1982) Single-neuron labeling in the cat auditory nerve. Science 216:1239–1241.

Liberman MC, Gao J, He DZ, Wu X, Jia S, Zuo J (2002) Prestin is required for electromotility of the outer hair cell and for the cochlear amplifier. Nature 419:300–304.

Lien CC, Jonas P (2003) Kv3 potassium conductance is necessary and kinetically optimized for high-frequency action potential generation in hippocampal interneurons. J Neurosci 23:2058–2068.

Lukashkin AN, Lukashkina VA, Russell IJ (2002) One source for distortion product otoacoustic emissions generated by low- and high-level primaries. J Acoust Soc Am 111:2740–2748.

Marcotti W, Johnson SL, Holley MC, Kros CJ (2003) Developmental changes in the expression of potassium currents of embryonic, neonatal and mature mouse inner hair cells. J Physiol (Lond) 548:383–400.

Marcotti W, Johnson SL, Kros CJ (2004) Effects of intracellular stores and extracellular Ca^{2+} on Ca^{2+}-activated K^+ currents in mature mouse inner hair cells. J Physiol (Lond) 557:613–633.

Mitra P, Slaughter MM (2002) Mechanism of generation of spontaneous miniature outward currents (SMOCs) in retinal amacrine cells. J Gen Physiol 119:355–372.

Moser T, Beutner D (2000) Kinetics of exocytosis and endocytosis at the cochlear inner hair cell afferent synapse of the mouse. Proc Natl Acad Sci USA 97:883–888.

Oliver D, Klocker N, Schuck J, Baukrowitz T, Ruppersberg JP, Fakler B (2000) Gating of Ca^{2+}-activated K^+ channels controls fast inhibitory synaptic transmission at auditory outer hair cells. Neuron 26:595–601.

Oliver D, Knipper M, Derst C, Fakler B (2003) Resting potential and submembrane calcium concentration of inner hair cells in the isolated mouse cochlea are set by KCNQ-type potassium channels. J Neurosci 23:2141–2149.

Palmer AR (2004) Reassessing mechanisms of low-frequency sound localisation. Curr Opin Neurobiol 14:457–460.

Palmer AR, Russell IJ (1986) Phase-locking in the cochlear nerve of the guinea-pig and its relation to the receptor potential of inner hair-cells. Hear Res 24:1–15.

Russell IJ, Sellick PM (1978) Intracellular studies of hair cells in the mammalian cochlea. J Physiol (Lond) 284:261–290.

Ruttiger L, Sausbier M, Zimmermann U, Winter H, Braig C, Engel J, Knirsch M, Arntz C, Langer P, Hirt B, Muller M, Kopschall I, Pfister M, Munkner S, Rohbock K, Pfaff I, Rusch A, Ruth P, Knipper M (2004) Deletion of the Ca^{2+}-activated potassium (BK) alpha-subunit but not the BKbeta1-subunit leads to progressive hearing loss. Proc Natl Acad Sci USA 101:12922–12927.

Sakaba T, Ishikane H, Tachibana M (1997) Ca^{2+}-activated K^+ current at presynaptic terminals of goldfish retinal bipolar cells. Neurosci Res 27:219–228.

Sausbier M, Hu H, Arntz C, Feil S, Kamm S, Adelsberger H, Sausbier U, Sailer CA, Feil R, Hofmann F, Korth M, Shipston MJ, Knaus HG, Wolfer DP, Pedroarena CM, Storm JF, Ruth P (2004) Cerebellar ataxia and Purkinje cell dysfunction caused by Ca^{2+}-activated K^+ channel deficiency. Proc Natl Acad Sci USA 101:9474–9478.

Sewell WF (1984) The relation between the endocochlear potential and spontaneous activity in auditory nerve fibres of the cat. J Physiol (Lond) 347:685–696.

Shao LR, Halvorsrud R, Borg-Graham L, Storm JF (1999) The role of BK-type Ca^{2+}-dependent K^+ channels in spike broadening during repetitive firing in rat hippocampal pyramidal cells. J Physiol (Lond) 521:135–146.

Shen Z, Liang F, Hazen-Martin DJ, Schulte BA (2004) BK channels mediate the voltage-dependent outward current in type I spiral ligament fibrocytes. Hear Res 187:35–43.

Siegel JH, Relkin EM (1987) Antagonistic effects of perilymphatic calcium and magnesium on the activity of single cochlear afferent neurons. Hear Res 28:131–147.

Skinner LJ, Enee V, Beurg M, Jung HH, Ryan AF, Hafidi A, Aran J-M, Dulon D (2003) Contribution of BK Ca^{2+}-activated K^+ channels to auditory neurotransmission in the guinea pig cochlea. J Neurophysiol 90:320–332.

Smith RL, Brachman ML, Goodman DA (1983) Adaptation in the auditory periphery. Ann NY Acad Sci 405:79–93.

Spassova MA, Avissar M, Furman AC, Crumling MA, Saunders JC, Parsons TD (2004) Evidence that rapid vesicle replenishment of the synaptic ribbon mediates recovery from short-term adaptation at the hair cell afferent synapse. J Assoc Res Otolaryngol 5:376–390.

Taberner AM, Liberman MC (2005) Response properties of single auditory nerve fibers in the mouse. J Neurophysiol 93:557–569.

Thurm H, Fakler B, Oliver D (2005) Ca^{2+}-independent activation of BK_{Ca} channels at negative potentials in mammalian inner hair cells. J Physiol (Lond) 569:137–151.

Vergara C, Latorre R, Marrion NV, Adelman JP (1998) Calcium-activated potassium channels. Curr Opin Neurobiol 8:321–329.

Vigh J, Solessio E, Morgans CW, Lasater EM (2003) Ionic mechanisms mediating oscillatory membrane potentials in wide-field retinal amacrine cells. J Neurophysiol 90:431–443.

Zeddies DG, Siegel JH (2004) A biophysical model of an inner hair cell. J Acoust Soc Am 116:426–441.